

Active nematics with quenched disorder

Sameer Kumar* and Shradha Mishra†

Indian Institute of Technology (BHU), Varanasi, U.P. India - 221005

In this study we introduce a two-dimensional active nematics with quenched disorder. We write the coarse-grained hydrodynamic equations of motion for slow variables, *viz.* density and orientation. Strength of disorder is tuned from zero to large values. Results from numerical solution of equations of motion and the calculation of two-point orientation correlation function using linear approximation, shows that the ordered steady state follows a disorder dependent crossover from quasi long range order (QLRO) to short range order (SRO). Such crossover is due to the pinning of $\pm 1/2$ topological defects in the presence of finite disorder, which breaks the system in uncorrelated domains. Finite disorder slows the dynamics of $+1/2$ defect, and it leads to slower growth dynamics. The two-point correlation functions for the density and the orientation fields, shows good dynamic scaling but no static scaling for the different disorder. Our findings can motivate experimentalists to verify the results and may find applications in living and artificial systems in the presence of a quenched impurity in active nematics.

Introduction: Dynamics and steady-state of a collection of active self-propelled particles with different kinds of inhomogeneities has become an active and interesting area of research [1–7]. Recent studies have mostly focused on the polar self-propelled particles in the presence of inhomogeneous agents/medium [8–10]. The effect of disorder in active polar particles introduces many interesting features, which, in general, not present in the corresponding equilibrium system of the same symmetry [11]. Study on the effect of disorder in apolar particles is limited to equilibrium system [12]. Disorder is present almost everywhere in active apolar systems [1], but ordering and steady state of active apolar particles with disorder is rarely studied.

Variety of systems where particles have head tail symmetry, like vibrated granular rods [13, 14], collection of molecular motors, cytoskeletal filaments [15, 16], mesenchymal, epithelial cells monolayers [17–20], bacterial colonies [21–23], and colonies of swarming filamentous bacteria [24] are a few examples of active apolar particles. Collection of such active apolar particles, forming an orientationally ordered state is called as *active nematics*. Most of the previous studies of active nematic are for clean system [25–28]. But, inhomogeneity or disorder can play a crucial role in steady-state and kinetics of active nematics, which is the focus of our current study.

In this letter, we study the effect of quenched disorder on a collection of active apolar particles on a two-dimensional substrate. The disorder is introduced as a random field of strength h_0 in the coarse-grained hydrodynamic equations of motion for slow variables; local density $\rho(\mathbf{r}, t)$ and order parameter $Q(\mathbf{r}, t)$. We first characterise the steady state and then study the ordering kinetics to the steady state. We calculate the nematic

order parameter (NOP) Q *vs.* system size N for different strength of disorder h_0 . For clean or homogeneous active nematic, NOP decay algebraically with N (quasi-long range order, QLRO). But for finite disorder, NOP shows a power-law decay, for small N and a disorder dependent crossover to an exponential decay (short-range order, SRO) for larger N and the result is supported by the calculation of two-point orientation correlation function in the steady state, using linear approximation. The origin of such crossover for the finite disorder ($h_0 \neq 0$), is due to the pinning of two-types of defects $\pm 1/2$. For large enough N , it breaks the system in uncorrelated domains and the size of these domains depends on the strength of the disorder. Although the orientation field is significantly affected due to disorder but, density fluctuation remains unaffected and shows the usual giant number fluctuation (GNF) [26, 27, 29] for all disorder (h_0).

We also studied the effect of disorder on the dynamics of the two types of defects and the ordering kinetics of the steady-state. Disorder in the system decreases the dynamics of $+1/2$ defect. The *effective* dynamic growth exponent, z_{eff} [30] increases on increasing disorder. The two-point correlation functions for both field shows a good dynamics scaling for all disorder, but no static scaling is found for different disorder.

Model: We construct a mono layer of self-propelled apolar particles of length l , moving on a two-dimensional substrate of friction coefficient χ . Each particle is driven by an internal force F acting along the long axis of the particle. The ratio of the force F to the friction coefficient gives a constant self-propulsion speed $v_0 = F/\chi$ to each particle. Apolar nature of the particle makes them move forward and backward with *equal* probability with a step size equal to their propulsion speed v_0 . On time scale, large compared to interaction time and length scale much larger than the particle size, the dynamics of the system is governed by coupled hydrodynamic equations of motion for slow variables *viz.* local density (which is obtained by calculating the num-

* sameerk.rs.phy16@itbhu.ac.in

† smishra.phy@itbhu.ac.in

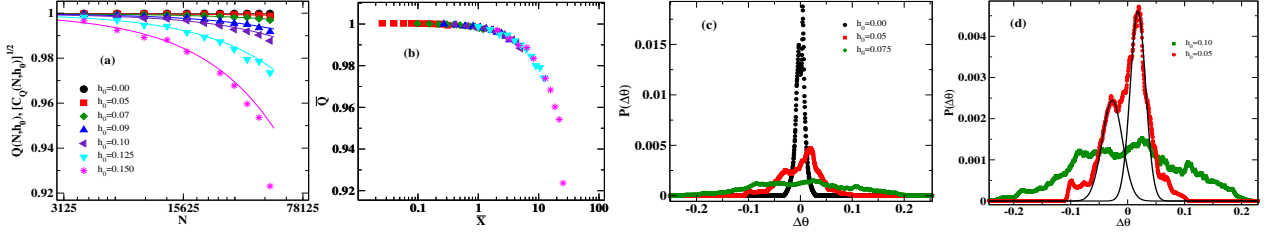


FIG. 1. (Color online) (a) Nematic Order parameter Q vs. system size $N = K \times K$ for different h_0 (symbols) and $\sqrt{C_Q}$, Eq. (3) (solid lines), (b) Scaled nematic OP, $\bar{Q} = Q \times N^{B'/2}$ vs. $\bar{X} = N \times h_0^4$. (c) Probability distribution function $P(\Delta\theta)$ of angle fluctuations for different value of h_0 . (d) Zoomed in $P(\Delta\theta)$ for $h_0 = 0.05$ (data points) fitted with Gaussian for two distinct peaks (solid lines) and $h_0 = 0.075$. $P(\Delta\theta)$ is calculated for $K = 500$.

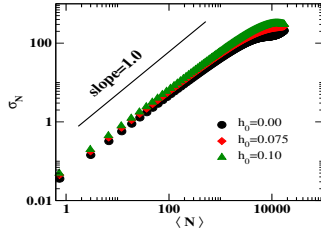


FIG. 2. (Color online) Number fluctuation σ_N vs. $\langle N \rangle$ plot for different disorder strengths for $K = 300$.

ber of particles in the coarse-grained region) $\rho(\mathbf{r}, t)$, and local nematic order parameter $Q(\mathbf{r}, t)$, defined as $Q_{ij} = \frac{\sum_{\alpha} \delta(\mathbf{r} - \mathbf{R}_{\alpha}(t)) (\hat{\mathbf{n}}_{\alpha,i} \hat{\mathbf{n}}_{\alpha,j} - \frac{1}{2} \delta_{ij})}{\rho(\mathbf{r}, t)}$, where \mathbf{R}_{α} is the position and $\hat{\mathbf{n}}_{\alpha}$ is the unit direction vector of the particle α , and $i, j = 1, 2$ in two-dimensions. The coarse-grained equation for $\rho(\mathbf{r}, t)$ is

$$\partial_t \rho = a_0 \nabla_i \nabla_j \rho Q_{ij} + D \rho \nabla^2 \rho \quad (1)$$

and the corresponding equation for $Q(\mathbf{r}, t)$ is

$$\partial_t Q_{ij} = [\alpha_1(\rho) - \alpha_2(Q : Q)] Q_{ij} + \beta (\nabla_i \nabla_j - \frac{1}{2} \delta_{ij} \nabla^2) \rho + D_Q \nabla^2 Q_{ij} + H_{ij} + \mathbf{f}_{\mathbf{R}} \quad (2)$$

The Eqs. (1) and (2) are written in dimensionless units by rescaling all lengths by the length of the particle and time by the collision time and are of the same form as derived from the microscopic rule based model in [25]. In Eq. (1), a_0 is the activity parameter and, $a_0 \propto v_0^2$. D_{ρ} is self diffusion term in density. First, two terms on the R. H. S. of Eq. (2) are the mean-field terms: where, $\alpha_1(\rho) = \alpha_0 (\frac{\rho}{\rho_c} - 1)$ where ρ_c is the critical density, where $\alpha_0 = 1$ is chosen as unity for simplicity. System shows homogeneous ordered state for $\alpha_1(\rho_0) > 0$, and disordered isotropic state when $\alpha_1(\rho_0) < 0$, where ρ_0 is the mean density of particles. The third term is coupling to the density field and the fourth term is the diffusion in Q . Origin of such diffusion can be obtained from the equal elastic constant approximation of Frank-free energy for two-dimensional equilibrium nematic [31, 32] and the last two terms are the *quenched disorder*, which is a new term introduced in our model, and the noise, respectively. The quenched disorder is introduced as *random field* in the free energy density $\mathcal{F} = -Q : \mathbf{h}\mathbf{h}$. Which further leads to $-(\mathbf{h}\mathbf{h} - \frac{1}{2}\mathbf{I})$ in equation 2. In two-dimensions $h_i = h_0(\cos\phi, \sin\phi)$, here h_0 is the disorder strength and $\phi(\mathbf{r})$ is a uniform random angle between $(0, 2\pi)$ with mean zero and space correlation $\langle \phi(\mathbf{r})\phi(\mathbf{r}') \rangle = \delta(\mathbf{r} - \mathbf{r}')$. The last term, $\mathbf{f}_{\mathbf{R}}(\mathbf{r}, t)$ is nonconserving spatiotemporal Gaussian

random white-noise with mean zero and noise-noise correlation $\langle f_i(\mathbf{r}, t) f_j(\mathbf{r}', t') \rangle = \Delta \delta_{ij} \delta(\mathbf{r} - \mathbf{r}') \delta(t - t')$ and Δ is the noise strength.

Random field introduced in our current model is similar to random field in XY-model (RFXY-model) [11]. Hereafter we refer our model as random field active nematic (RF-active nematic) when $h_0 \neq 0$, and clean-active nematic (clean-AN) for $h_0 = 0$.

To perform the numerical integration of Eqs. 1 and 2 we construct a two-dimensional $K \times K$ square lattice with periodic boundary condition (PBC) and discretise the space and time derivatives using Euler scheme ($\Delta x = 1.0$ and $\Delta t = 0.1$). Initially, we start with random homogeneous density with mean ($\rho_0 = 0.75$) and random direction of the orientation field.

We first study the steady-state of the system for different strength of disorder $h_0 = (0.0, 0.15)$ and different system size, i.e. $K = 64$ to 512. Coarsening is studied for larger $K = 1024$. Steady-state results are obtained for simulation time $t = \mathcal{O}(10^6)$ and the average over 10 independent realisations. One simulation time is counted after update of Eqs. 1 and 2 for all lattice points $K \times K$. The strength of random noise is fixed $\Delta = 10^{-4}$ and other parameters in Eqs. (1) and (2) are $a_0 = 0.2$, $\rho_0 = 0.75$, $\rho_c = 0.5$, $\alpha_2 = 1$, $\beta = 0.25$, $D_{\rho} =$

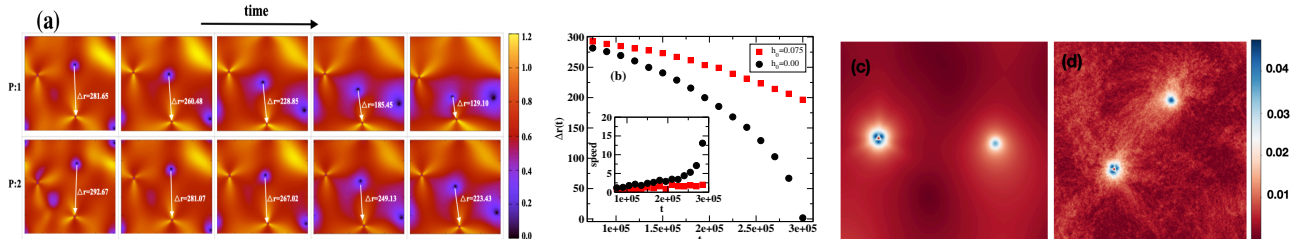


FIG. 3. (Color online) (a) Snapshots of local nematic OP \mathcal{Q} : upper panel (P:1) is for clean-AN (i.e. $h_0 = 0.0$) and bottom panel (P:2) is for RF-active nematic ($h_0 = 0.075$) and the number along the white arrow is the length of the arrow which is equal to relative separation ($\Delta r(t)$) between the $\pm 1/2$ defects. (b) $\Delta r(t)$ vs. t plot for $h_0 = 0.0, 0.075$. Inset figure shows the relative speeds of $\pm 1/2$ defects. Data is generated for system size $K = 512$. (c) Snapshot of density current near the defects for clean system, $h_0 = 0.0$ and (d) with disorder, $h_0 = 0.075$. Intensity of colors shows the magnitude of the density current.

0.26 and $D_{\mathcal{Q}} = 1$ and we check that, system remains stable for the chosen set of parameters.

Results:-

We first measure the ordering in the RF-active nematic in the steady state for different strength of disorder h_0 . The global ordering in the system is measured by calculating the nematic order parameter (NOP) defined as

$\mathbf{Q} = \langle \frac{1}{N} \sqrt{|\sum_{i=1}^N \cos(2\theta_i)|^2 + |\sum_{i=1}^N \sin(2\theta_i)|^2} \rangle$, where $N = K^2$ is the size of the system, and $\theta_i(t)$ is the local orientation at i^{th} position on a two-dimensional lattice of size K . $\langle \dots \rangle$ shows the averaging over many realisations. We compare the measured \mathbf{Q} in numerical simulation with approximate analytic expression for the two-point orientation correlation function $C_{\mathcal{Q}}$, obtained from a linearised treatment of small fluctuation about a mean uniform ordered phase. We calculate the equal time Fourier transformed spatial correlation of angle $S_{\mathbf{q}}(\theta)$ as a function of wavevector \mathbf{q} and present our result for $q_x = q_y$. Starting from the equations of motion 1 and 2, a straight forward linearised approximation (detail calculation is given in the Appendix A) shows that for a finite strength of disorder,

$$C_{\mathcal{Q}}(N) \simeq \frac{1}{N^{\mathcal{B}'}} e^{-\mathcal{C}' h_0^4 N} \quad (3)$$

which is obtained from the inverse Fourier transform of orientation structure factor $S_{\mathbf{q}}(\theta)$ at wave-number $q \simeq N^{-1/2}$. The full expression for \mathcal{B}' and \mathcal{C}' is given in Eq. A21 in the Appendix A, and are constants which depends on the chosen parameters in the system. For the chosen set of parameters in our present study $\mathcal{B}' = 1.17 \times 10^{-4}$ and $\mathcal{C}' = 3.9 \times 10^{-3}$. Hence $C_{\mathcal{Q}}$ is product of algebraic and exponential decay with N . Algebraic decay exponent \mathcal{B}' is independent of disorder and exponential decay sharpens with increasing h_0 . Fig. 1(a), data points shows the plot of NOP vs. N for different strength of disorder h_0 . For clean-AN, \mathbf{Q} decays algebraically as $N^{-\mathcal{B}'}$, where $\mathcal{B}' = \mathcal{O}(10^{-4})$ is small. This is because for the chosen set of parameters, clean-AN is in the deep ordered state and significantly away from the

isotropic-nematic transition, where it shows the instability [33–36]. For finite disorder, \mathbf{Q} shows the deviation from the pure algebraic decay. It decays algebraically for small N and shows a crossover to exponential decay for larger N . Larger the strength of disorder, the crossover to exponential decay appears for smaller N .

In Fig. 1(a) lines are plot of $\sqrt{C_{\mathcal{Q}}(N, h_0)}$, Eq. (3). For clean-AN, $C_{\mathcal{Q}}(N, 0)$ is pure power-law whereas, for RF-active nematic, it decays exponentially for higher N . Hence crossover happens after a disorder dependent N , $N_c(h_0) \sim h_0^{-4}$. We find a good match of lines (from linear approximation) and data from the numerical solution. A systematic deviation found for large N and h_0 , which is due to nonlinearities present in the model. In Fig. 1(b) we plot the $\mathbf{Q} \times N^{\mathcal{B}'/2}$ vs. $N \times h_0^4$ for different h_0 and find nice collapse of data for different disorder strengths.

To further understand the steady state in RF-active nematic, we plot the probability distribution function (PDF) $P(\Delta\theta)$ of angle fluctuations $\Delta\theta$ from the mean direction. Fig. 1(c) shows the plot of $P(\Delta\theta)$ vs. $\Delta\theta$ for $h_0 = 0.0, 0.05, 0.075$. $P(\Delta\theta)$ for clean-AN shows a very narrow peak at $\Delta\theta = 0$, whereas, for RF-active nematic, PDF clearly have more than one peak with non-zero $\Delta\theta$. Zoomed in plot is shown in Fig. 1(d) where, we plot $P(\Delta\theta)$ vs. $\Delta\theta$ for RF-active nematic (for $h_0 = 0.05, 0.075$) and fit to two distinct peaks for $h_0 = 0.05$ with Gaussian. Similarly for larger disorder, $P(\Delta\theta)$ shows larger number of such different peaks, which means that if we further increase the disorder strength, more number of ordered domains present in the system.

We also calculate the steady-state density fluctuation and find that for all disorder, number fluctuation $\sigma_{\mathcal{N}} = \sqrt{\langle \mathcal{N}^2 \rangle - \langle \mathcal{N} \rangle^2} \sim \langle \mathcal{N} \rangle$, where \mathcal{N} is the mean number of particle in subcell, Fig. 2, which shows a giant number fluctuation (GNF), as found in [26, 27, 29]. When compared with the linearised calculation of two-point density structure factor, as given in Eq. A33, for $q \simeq N^{-1/2}$, density fluctuation should show the fluctuations larger than the clean AN. But large fluctuation can arise for size $\mathcal{N} > \mathcal{N}_c \simeq h_0^4$,

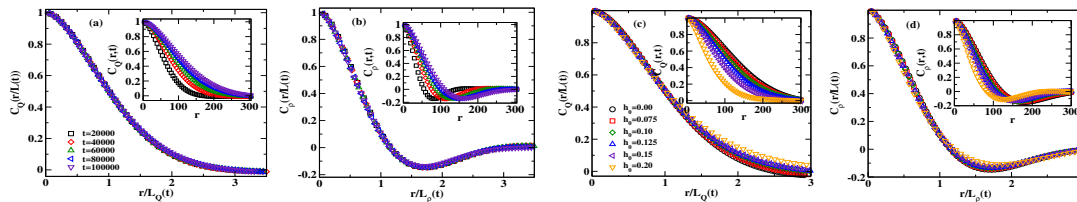


FIG. 4. (Color online) Plot of two-point correlation functions: (a-b) Scaled orientation-density correlation function $C_{\mathcal{Q},\rho}(r/L_{\mathcal{Q},\rho}(t))$ vs. scaled distance $r/L_{\mathcal{Q},\rho}(t)$ (main) and $C_{\mathcal{Q},\rho}(r,t)$ vs. r (inset); for $h_0 = 0.1$ at different simulation time (t). (c-d) Scaled orientation-density correlation function $C_{\mathcal{Q},\rho}(r/L_{\mathcal{Q},\rho}(t))$ vs. scaled distance $r/L_{\mathcal{Q},\rho}(t)$ (main) and $C_{\mathcal{Q},\rho}(r,t)$ vs. r (inset) at $t = 10^5$ and different h_0 . All data are for $K = 1024$.

which is hard to achieve in numerical simulation. Hence in general inhomogeneity does not affect the density fluctuations in active nematic, although it significantly changes the nature of two-point orientation correlation function. Now we further study the ordering kinetics to such steady state.

Kinetics:- When the system brought from a disordered state to an ordered state, ordering happens through the process of domain formation and which is due to the creation and annihilation of $\pm 1/2$ topological defects. In two-dimensional active nematic, these defects are not a point like objects but have topological geometry [37]. A $+1/2$ defect has a comet-like structure and moves along the axis parallel to its tail, whereas, a $-1/2$ defect have a three-fold symmetry and do not have any preferred direction of motion [38, 39]. The dynamics of defects play a vital role in the ordering of the system [30]. In Fig. 3(a-b), we study the dynamics of defects for a clean-AN ($h_0 = 0.0$) as well for RF-active nematic ($h_0 = 0.075$). Fig. 3(a) shows the snapshots of local NOP, \mathcal{Q} , for clean-AN (upper panel) and RF-active nematic (lower panel). White arrow shows the relative separation, $\Delta r(t)$, between a pair of $\pm 1/2$ defects. Tail and head of the arrow represents the position of $+1/2$ and $-1/2$ defects respectively. Relative motion of $+1/2$ defect has become slow in the presence of finite disorder. The variation of $\Delta r(t)$ vs. time is shown in Fig. 3(b). The length of the white arrow in Fig. 3(a) decreases with time (or Δr decay with time Fig. 3(b)), which shows the two defects come close to each other. For clean-AN, $\Delta r(t)$ decay at a faster rate whereas it takes a longer time in the presence of disorder. Hence the relative speed is small in the presence of disorder as shown in the inset of Fig. 3(b). To further understand the mechanism of slowing down of defect dynamics, in Fig. 3(c-d), we show the snapshot of the local density current near a pair of $\pm 1/2$ defects. Density current \mathbf{J}_ρ defined from Eq. (1), which can be rewritten as continuity equation, $\partial_t \rho = -\nabla \cdot \mathbf{J}_\rho$ where $\mathbf{J}_\rho = -\nabla(a_0 \rho \mathcal{Q} + D_\rho \rho)$. The intensity of colors shows the magnitude of the density current. For clean-AN, current flow is smooth near the defects Fig. 3(c), whereas with disorder ($h_0 = 0.075$), current flow is distorted, Fig. 3(d), which results a slower growth dynamics, we will discuss next.

Growth law and scaling behaviour: As we discussed in

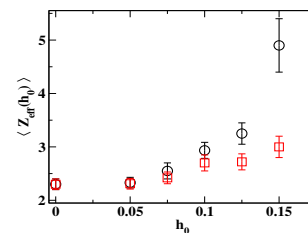


FIG. 5. (Color online) Plot of dynamic growth exponent z_{eff} vs. disorder strength h_0 . Circles are the data for $z_{eff,\mathcal{Q}}$ and squares are data for $z_{eff,\rho}$ for $K = 1024$

previous paragraph, disorder affect the defect dynamics, and it can further influence the kinetics of domain ordering. We characterise the domain growth by calculating the correlation functions for orientation \mathcal{Q} , $C_{\mathcal{Q}}(\mathbf{r}, t) = \langle \mathcal{Q}(\mathbf{0}, t) : \mathcal{Q}(\mathbf{r}, t) \rangle$ and, local density ρ , $C_\rho(\mathbf{r}, t) = \langle \delta\rho(\mathbf{0}, t), \delta\rho(\mathbf{r}, t) \rangle$, where $\delta\rho(\mathbf{r}, t) = \rho(\mathbf{r}, t) - \rho_0$ is the deviation of the local density from the mean ρ_0 . With time both correlations increases due to domain growth. In Fig. 4(a-d) (insets) we plot the two correlation functions ($C_{\mathcal{Q}}$ and C_ρ) vs. distance r . Fig. 4(a-b)(main) show the plot of $C_{\mathcal{Q}}(r/L(t))$ and $C_\rho(r/L(t))$ vs. scaled distance $r/L_{\mathcal{Q},\rho}(t)$ and they all collapse to single curve. Where the characteristic length $L_{\mathcal{Q},\rho}(t)$ is calculated from the first zero crossing of $C_{\mathcal{Q}}(\mathbf{r}, t)$ and $C_\rho(\mathbf{r}, t)$. Fig. 4(c-d)(main) shows the plot of $C_{\mathcal{Q},\rho}(r/L(t))$ and $C_{\rho,r}(r/L(t))$ vs. scaled distance $r/L_{\mathcal{Q},\rho}(t)$ calculated at equal simulation time ($t = 100000$) for different disorder h_0 . We find no scaling for different disorder for both \mathcal{Q} and ρ . Therefore, for all disorder system shows good dynamic scaling but no static scaling in orientation and density.

We further calculate the dynamics growth exponent $z_{eff,\mathcal{Q},\rho}$ defined as $\frac{1}{z_{eff,\mathcal{Q},\rho}} = \langle \frac{d \ln L_{\mathcal{Q},\rho}(t)}{d(t/\ln t)} \rangle$ [30], where $\langle \dots \rangle$ is mean value of z_{eff} over intermediate time when it remains constant for at least one decade. We find that $z_{eff,\mathcal{Q},\rho} \simeq 2$ for Clean-AN and increases on increasing h_0 , but change in $z_{eff,\rho}$ is relatively small in comparison to $z_{eff,\mathcal{Q}}$. Hence although disorder affect orientation ordering substantially but density field is not much affected.

We also measure the effect of disorder on domain morphology by estimating the cusp exponent, α , (details

given in the Appendix B), In clean-AN as well as RF-active nematic $\alpha \simeq 1.7$ for all disorder strength and both fields. Hence disorder although slows the domain growth but morphology of ordered domains remains unchanged.

Discussion:- We studied a two-dimensional active nematics with the quenched random field and write the hydrodynamic equations of motion for the hydrodynamics fields, *viz.* density ρ and orientation Q , in a coarse-grained description.

The study from numerical solution of equations of motion and the linearized hydrodynamic calculation shows that the orientation correlation follows a crossover from QLRO (algebraic decay of correlation) to SRO (exponential decay). Such crossover occurs due to pinning of $\pm 1/2$ defects in the presence of finite disorder, which breaks the system in domains of different orientation. Size of such domains decreases on increasing disorder. For clean as well as RF-active nematic, number fluctuation $\Delta N \sim \mathcal{N}$.

We also studied the approach to the steady state by (i) characterizing the dynamics of $\pm 1/2$ defects and (ii) calculation of the characteristic length of growing domains $L_{Q,\rho}(t)$. The slow dynamics of $+1/2$ defect leads

to the slower domain growth in the presence of disorder.⁵ Although domain growth is slower in the presence of disorder, but the two-point correlation function for both fields $C_{\rho,Q}$ shows good dynamic scaling, but no static scaling is found for fixed time and different disorder. Domain morphology remains unaffected in the presence of disorder.

Hence our study shows an interesting steady state in RF-active nematic, which is different from its corresponding equilibrium analogue: random field XY-model [11]. Our study should motivate experimentalist to verify our findings as well as encourages to study the effect of other kinds of disorder in active nematics.

SM would like to thank Sriram Ramaswamy and Sanjay Puri for useful discussion at the beginning of the project. SK would like to thank Rajeev Singh for useful suggestions. SM and SK, thanks DST-SERB India, ECR/2017/000659 for partial financial support.

I. REFERENCES

-
- [1] C. J. O. Reichhardt and C. Reichhardt, *Nature Physics* **13** (2017).
 - [2] A. Morin, N. Desreumaux, J. B. Caussin, and D. Bartolo, *Nature Physics* **13**, 63 (2017), arXiv:1610.04404.
 - [3] R. Das, M. Kumar, and S. Mishra, *Physical Review E* **98**, 2 (2018), arXiv:1802.08861.
 - [4] J. Toner, N. Guttenberg, and Y. Tu, *Physical Review Letters* **121**, 248002 (2018), arXiv:1805.10324.
 - [5] J. Toner, N. Guttenberg, and Y. Tu, *Physical Review E* **98**, 1 (2018), arXiv:1805.10326.
 - [6] O. Chepizhko, E. G. Altmann, and F. Peruani, *Physical Review Letters* **110**, 1 (2013), arXiv:1305.5707.
 - [7] A. Maitra, *Physical Review E* **101**, 1 (2020), arXiv:1910.07334.
 - [8] C. Dombrowski, L. Cisneros, S. Chatkaew, R. E. Goldstein, and J. O. Kessler, *Physical Review Letters* **93**, 2 (2004).
 - [9] T. Sanchez, D. T. Chen, S. J. Decamp, M. Heymann, and Z. Dogic, *Nature* **491**, 431 (2012).
 - [10] Y. Sumino, K. H. Nagai, Y. Shitaka, D. Tanaka, K. Yoshikawa, H. Chaté, and K. Oiwa, *Nature* **483**, 448 (2012).
 - [11] Y. Imry and S. K. Ma, *Physical Review Letters* **35**, 1399 (1975).
 - [12] M. Rotunno, M. Buscaglia, C. Chiccoli, F. Mantegazza, P. Pasini, T. Bellini, and C. Zannoni, *Physical Review Letters* **94**, 1 (2005).
 - [13] D. L. Blair, T. Neicu, and A. Kudrolli, *Physical Review E - Statistical Physics, Plasmas, Fluids, and Related Interdisciplinary Topics* **67**, 6 (2003), arXiv:0203236 [cond-mat].
 - [14] A. Sokolov, I. S. Aranson, J. O. Kessler, and R. E. Goldstein, *Physical Review Letters* **98**, 1 (2007).
 - [15] R. Komkemer, D. Kling, D. Kaufmann, and H. Gruler, *European Physical Journal E* **1**, 215 (2000).
 - [16] L. H. Cisneros, J. O. Kessler, S. Ganguly, and R. E. Goldstein, *Physical Review E - Statistical, Nonlinear, and Soft Matter Physics* **83**, 1 (2011).
 - [17] G. Duclos, C. Erlenkämper, J. F. Joanny, and P. Silberzan, *Nature Physics* **13**, 58 (2017).
 - [18] K. Kawaguchi, R. Kageyama, and M. Sano, *Nature* **545**, 327 (2017).
 - [19] T. B. Saw, A. Doostmohammadi, V. Nier, L. Kocgozlu, S. Thampi, Y. Toyama, P. Marcq, C. T. Lim, J. M. Yeomans, and B. Ladoux, *Nature* **544**, 212 (2017).
 - [20] C. Blanch-Mercader, V. Yashunsky, S. Garcia, G. Duclos, L. Giomi, and P. Silberzan, *Physical Review Letters* **120**, 208101 (2018), arXiv:1711.01568.
 - [21] A. Doostmohammadi, S. P. Thampi, and J. M. Yeomans, *Physical Review Letters* **117**, 1 (2016), arXiv:1601.04489.
 - [22] D. Dell’Arciprete, M. L. Blow, A. T. Brown, F. D. Farrell, J. S. Lintuvuori, A. F. McVey, D. Marenduzzo, and W. C. Poon, *Nature Communications* **9**, 1 (2018).
 - [23] Y. I. Yaman, E. Demir, R. Vetter, and A. Kocabas, *Nature Communications* **10**, 1 (2019), arXiv:1811.12076.
 - [24] H. Li, X. qing Shi, M. Huang, X. Chen, M. Xiao, C. Liu, H. Chaté, and H. P. Zhang, *Proceedings of the National Academy of Sciences of the United States of America* **116**, 777 (2019).
 - [25] E. Bertin, H. Chaté, F. Ginelli, S. Mishra, A. Peshkov, and S. Ramaswamy, *New Journal of Physics* **15** (2013), 10.1088/1367-2630/15/8/085032, arXiv:1305.0772.
 - [26] H. Chaté, F. Ginelli, and R. Montagne, *Physical Review Letters* **96**, 1 (2006), arXiv:0603080 [cond-mat].
 - [27] S. Ramaswamy, R. A. Simha, and J. Toner, *Europhysics*

- Letters **62**, 196 (2003), arXiv:0208573 [cond-mat].
- [28] A. Doostmohammadi, J. Ignés-Mullol, J. M. Yeomans, and F. Sagués, *Nature Communications* **9** (2018), 10.1038/s41467-018-05666-8.
- [29] S. Mishra and S. Ramaswamy, *Physical Review Letters* **97**, 1 (2006), arXiv:0603051 [cond-mat].
- [30] A. J. Bray, *Advances In Physics* **43**, 357 (1994).
- [31] P. M. Chaikin and T. C. Lubensky, Cambridge University Press (1995).
- [32] P. G. de Gennes and J. Prost, Clarendon Press (1993).
- [33] X.-q. Shi and Y.-q. Ma, (2010), arXiv:1011.5408.
- [34] R. Das, M. Kumar, and S. Mishra, *Scientific Reports* **7**, 1 (2017).
- [35] X. Q. Shi and Y. Q. Ma, *Nature Communications* **4**, 1 (2013).
- [36] X. Q. Shi, H. Chaté, and Y. Q. Ma, *New Journal of Physics* **16** (2014), 10.1088/1367-2630/16/3/035003.
- [37] A. J. Vromans and L. Giomi, *Soft Matter* **12**, 6490 (2016), arXiv:1507.05588.
- [38] N. M. Vijay Narayan, Sriram Ramaswamy, *Science* **317**, 105 (2007).
- [39] S. Mishra, S. Puri, and S. Ramaswamy, *Philosophical Transactions of the Royal Society A: Mathematical*

ical, Physical and Engineering Sciences **372** (2014)⁶, 10.1098/rsta.2013.0364.

- [40] G. B. Arfken and H. J. Weber, *Mathematical Methods for Physics* (ELSEVIER Academic Press, 2012) pp. 675–739.

Appendix A: Linearised hydrodynamic calculation of two-point correlation functions

We rewrite Eqs. (1) and (2) neglecting the higher order fluctuations about the homogeneous ordered steady state. The local nematic order parameter \mathcal{Q} is given as $\mathcal{Q} = \frac{S}{2} \begin{bmatrix} \cos 2\theta & \sin 2\theta \\ \sin 2\theta & -\cos 2\theta \end{bmatrix}$ where, S is a scalar and a measure of ordering. We define $\delta\rho$, δS and θ as the fluctuation terms from their mean values ρ_0 , S_0 and θ_0 respectively. Here, $S_0 = \sqrt{\frac{2\alpha_1(\rho_0)}{\alpha_2}}$, and is obtained from Eq. (2) for homogeneous steady state. Therefore, in linear order we have $\mathcal{Q}_{11} = \frac{1}{2}(S_0 + \delta S)$, $\mathcal{Q}_{12} = \theta S_0$.

To linear order, Eq. (1) gives,

$$\partial_t(\rho_0 + \delta\rho) = a_0[\partial_x^2(\rho_0 + \delta\rho)\frac{(S_0 + \delta S)}{2} + \partial_y^2(\rho_0 + \delta\rho)\frac{-(S_0 + \delta S)}{2} + 2\partial_x\partial_y(\rho_0 + \delta\rho)S_0\theta] + D_\rho\nabla^2(\rho_0 + \delta\rho) \quad (\text{A1})$$

or,

$$\partial_t\delta\rho = a_0[(\partial_x^2\frac{(S_0\delta\rho + \rho_0\delta S)}{2} - \partial_y^2\frac{(S_0\delta\rho + \rho_0\delta S)}{2} + 2S_0\rho_0\partial_x\partial_y\theta] + D_\rho(\partial_x^2 + \partial_y^2)\delta\rho \quad (\text{A2})$$

or,

$$\partial_t\delta\rho = (\frac{a_0S_0}{2} + D_\rho)\partial_x^2\delta\rho + (D_\rho - \frac{a_0S_0}{2})\partial_y^2\delta\rho + \frac{a_0\rho_0}{2}(\partial_x^2 - \partial_y^2)\delta S + 2a_0\rho_0S_0\partial_x\partial_y\theta \quad (\text{A3})$$

while, the equation for δS (Eq. (2)) in homogeneous steady state gives,

$$0 = [\alpha_1(\rho_0) + \alpha_1'(\rho_0)\delta\rho - \frac{\alpha_2}{2}(S_0^2 + 2S_0\delta S)]\frac{S_0 + \delta S}{2} + \dots \quad (\text{A4})$$

also, $\alpha_1(\rho_0) - \frac{\alpha_2}{2}S_0^2 = 0$. Therefore we have,

$$(\alpha_1'(\rho_0)\delta\rho - \alpha_2S_0\delta S)(S_0 + \delta S) = 0 \quad (\text{A5})$$

$$\delta S = \frac{\alpha_1'(\rho_0)\delta\rho}{\alpha_2S_0} \quad (\text{A6})$$

or,

$$\delta S = \Gamma\delta\rho \quad (\text{A7})$$

where, $\Gamma = \frac{\alpha_1'(\rho_0)}{\alpha_2S_0}$ and $\alpha_1' = \frac{\partial\alpha_1(\rho)}{\partial\rho}|_{\rho=\rho_0}$. Hence, Eq. (A3) can be re-written as,

$$\partial_t\delta\rho = (\frac{a_0S_0}{2} + D_\rho)\partial_x^2\delta\rho + (D_\rho - \frac{a_0S_0}{2})\partial_y^2\delta\rho + \frac{a_0\rho_0}{2}\Gamma(\partial_x^2 - \partial_y^2)\delta\rho + 2a_0\rho_0S_0\partial_x\partial_y\theta \quad (\text{A8})$$

or,

$$\partial_t\delta\rho = (\frac{a_0S_0}{2} + D_\rho + \Gamma\frac{a_0\rho_0}{2})\partial_x^2\delta\rho + (-\frac{a_0S_0}{2} + D_\rho - \Gamma\frac{a_0\rho_0}{2})\partial_y^2\delta\rho + 2a_0\rho_0S_0\partial_x\partial_y\theta \quad (\text{A9})$$

or,

$$\partial_t \delta \rho = K_1 \partial_x^2 \delta \rho + K_2 \partial_y^2 \delta \rho + K_3 \partial_x \partial_y \theta \quad (\text{A10})$$

Where, $K_1 = (\frac{a_0 S_0}{2} + D_\rho + \Gamma \frac{a_0 \rho_0}{2})$, $K_2 = (-\frac{a_0 S_0}{2} + D_\rho - \Gamma \frac{a_0 \rho_0}{2})$ and $K_3 = 2a_0 \rho_0 S_0$.

Now the equation of motion for \mathcal{Q}_{12} ,

$$\partial_t \mathcal{Q}_{12} = [\alpha_1(\rho) - \alpha_2(\mathcal{Q} : \mathcal{Q})] \mathcal{Q}_{12} + \beta(\nabla_1 \nabla_2 - \frac{1}{2} \delta_{12} \nabla^2) \rho + D_{\mathcal{Q}} \nabla^2 \mathcal{Q}_{12} + H_{12} + \mathbf{f}_{\mathbf{R}} \quad (\text{A11})$$

Here, $\mathcal{Q}_{12} = S_0 \theta$ therefore, in linear order, $[\alpha_1(\rho) - \alpha_2(\mathcal{Q} : \mathcal{Q})] \mathcal{Q}_{12}$ will not survive. $h_1 h_2 = h_0^2 \cos \phi \sin \phi = h_0^2 \Phi(\mathbf{r})$, wherec $\Phi(\mathbf{r}) = \cos \phi \sin \phi$.

$$\partial_t \theta = \frac{\beta}{\rho_0 S_0} \partial_x \partial_y \delta \rho + D_{\mathcal{Q}} (\partial_x^2 + \partial_y^2) \theta + \frac{h_0^2}{\rho_0 S_0} \Phi + \frac{1}{\rho_0 S_0} \mathbf{f}_{\mathbf{R}} \quad (\text{A12})$$

Taking the Fourier transform of equation (A10) and (A12), where Fourier modes are defined as, $f(\mathbf{q}, \omega) = \int \int f(\mathbf{r}, t) e^{i\mathbf{q} \cdot \mathbf{r} + i\omega t} d\mathbf{r} dt$, we get,

$$(K_1 q_x^2 + K_2 q_y^2 - i\omega) \delta \rho(\mathbf{q}, \omega) + K_3 q_x q_y \theta(\mathbf{q}, \omega) = 0 \quad (\text{A13})$$

and,

$$\frac{\beta}{\rho_0 S_0} q_x q_y \delta \rho(\mathbf{q}, \omega) + [D_{\mathcal{Q}} (q_x^2 + q_y^2) - i\omega] \theta(\mathbf{q}, \omega) = \frac{h_0^2}{\rho_0 S_0} \Phi(\mathbf{q}) + \frac{1}{\rho_0 S_0} \mathbf{F}_{\mathbf{R}}(\mathbf{q}, \omega) \quad (\text{A14})$$

Solving equation (A13) and (A14) will give,

$$\mathbf{M} \begin{bmatrix} \delta \rho(\mathbf{q}, \omega) \\ \theta(\mathbf{q}, \omega) \end{bmatrix} = \frac{1}{\rho_0 S_0} \begin{bmatrix} 0 \\ h_0^2 \Phi(\mathbf{q}) + \mathbf{F}_{\mathbf{R}}(\mathbf{q}, \omega) \end{bmatrix} \quad (\text{A15})$$

where,

$$\mathbf{M} = \begin{bmatrix} K_1 q_x^2 + K_2 q_y^2 - i\omega & K_3 q_x q_y \\ \frac{\beta}{\rho_0 S_0} q_x q_y & D_{\mathcal{Q}} (q_x^2 + q_y^2) - i\omega \end{bmatrix} \quad (\text{A16})$$

by solving equation (A15) for $q_x = q_y$, we get

$$\begin{bmatrix} \delta \rho(\mathbf{q}, \omega) \\ \theta(\mathbf{q}, \omega) \end{bmatrix} = \frac{1}{(D_1 q^4 + \omega^2) - i\omega D_2 q^2} \begin{bmatrix} -K_3 q^2 \\ 2D_\rho q^2 - i\omega \end{bmatrix} \frac{(h_0^2 \Phi(\mathbf{q}) + \mathbf{F}_{\mathbf{R}}(\mathbf{q}, \omega))}{\rho_0 S_0} \quad (\text{A17})$$

where, $D_1 = 4D_\rho D_{\mathcal{Q}} + 2a_0 \beta$ and $D_2 = 2(D_\rho + D_{\mathcal{Q}})$. Equation (A17) gives,

$$\delta \rho(\mathbf{q}, \omega) = \frac{-K_3 q^2}{(D_1 q^4 + \omega^2) - i\omega D_2 q^2} \frac{(h_0^2 \Phi(\mathbf{q}) + \mathbf{F}_{\mathbf{R}}(\mathbf{q}, \omega))}{\rho_0 S_0} \quad (\text{A18})$$

$$\theta(\mathbf{q}, \omega) = \frac{2D_\rho q^2 - i\omega}{(D_1 q^4 + \omega^2) - i\omega D_2 q^2} \frac{(h_0^2 \Phi(\mathbf{q}) + \mathbf{F}_{\mathbf{R}})}{\rho_0 S_0} \quad (\text{A19})$$

Now, we first calculate the two point orientation correlation functions,

$$\langle \theta(\mathbf{q}, \omega) \theta(-\mathbf{q}, -\omega) \rangle = \frac{D_\rho^2 q^4 + \omega^2}{(D_1 q^4 + \omega^2)^2 + \omega^2 D_2^2 q^4} \frac{[h_0^4 \langle \Phi(\mathbf{q}) \Phi(-\mathbf{q}) \rangle + \langle \mathbf{F}_{\mathbf{R}}(\mathbf{q}, \omega) \mathbf{F}'_{\mathbf{R}}(-\mathbf{q}, -\omega) \rangle]}{\rho_0 S_0} \quad (\text{A20})$$

here, $\langle \Phi(\mathbf{q}) \Phi(-\mathbf{q}) \rangle = \delta_{ij} \delta(\mathbf{q} + \mathbf{q})$ and $\langle \mathbf{F}_{\mathbf{R}}(\mathbf{q}, \omega) \mathbf{F}'_{\mathbf{R}}(-\mathbf{q}, -\omega) \rangle = \Delta \delta(\mathbf{q} + \mathbf{q}) \delta(\omega + \omega)$. Using this we get,

$$S_q(\theta) = \mathcal{C}(D_\rho, D_{\mathcal{Q}}) \frac{h_0^4}{q^4} + \mathcal{B}(D_\rho, D_{\mathcal{Q}}) \frac{1}{q^2} \quad (\text{A21})$$

Where, $\mathcal{C}(D_\rho, D_Q) = \frac{4D_\rho^2}{\rho_0 S_0 (4D_\rho D_Q + 2a_0\beta)^2}$ and $\mathcal{B}(D_\rho, D_Q) = \frac{\pi\Delta}{2\rho_0 S_0} \frac{1}{c\sqrt{2(4b^2+c^2)}} \left[\frac{(2a^2+c(\sqrt{4b^2+c^2})-2b^2)}{\sqrt{c(c-\sqrt{4b^2+c^2})+2b^2}} \right]$ where $a = D_\rho$, $b = \sqrt{2(2D_\rho D_Q + a_0\beta)}$ and $c = \sqrt{2(D_\rho + D_Q)}$.

Hence, the two point angle correlation function can be written as,

$$S_q(\theta) \simeq \frac{\mathcal{B}}{q^2} + \frac{Ch_0^4}{q^4} \quad (\text{A22})$$

Here, the coefficients \mathcal{C} and \mathcal{B} depends on system parameters. To get the two point correlation function for nematic order parameter $C_Q(x) \simeq \exp(-G_\theta(x))$ [31], where $G_\theta(x)$ is the inverse Fourier transform of $S_q(\theta)$ Eq. (A22). Also, $G(x) = \mathcal{B}f(x) + Ch_0^4 g(x)$, where,

$$f(x) = \int_{2\pi/L}^{2\pi/a} \frac{d^2q}{4\pi^2} \frac{1-e^{i\mathbf{q}\cdot\mathbf{x}}}{q^2} \simeq \ln(\Lambda|x|) \quad (\text{A23})$$

and,

$$g(x) = \int_{2\pi/a}^{2\pi/L} \frac{dq}{q^3} \left[\frac{1}{2} \int_0^{2\pi} d\theta (1 - e^{iq|x|\cos\theta}) \right] \quad (\text{A24})$$

or,

$$g(x) = \int_{2\pi/a}^{2\pi/L} \frac{dq}{q} (1 - J_0(q|x|)) \quad (\text{A25})$$

here, J_n is the n^{th} order Bessel's function [40].

$$g(x) = |x|^2 \int_0^1 \frac{du(1-J_0(u))}{u^3} + |x|^2 \int_1^{\Lambda|x|} \frac{du}{u^3} - |x|^2 \int_1^{\Lambda|x|} \frac{du J_0(u)}{u^3} \quad (\text{A26})$$

$$g(x) = |x|^2 A + |x|^2 \left[-\frac{1}{2} \left(1 - \frac{1}{\Lambda^2|x|^2} \right) \right] - |x|^2 \int_1^{2\pi/a|x|} \frac{du J_0(u)}{u^3} \quad (\text{A27})$$

$$g(x) = |x|^2 \left(A - \frac{1}{2} - |x|^2 \int_1^{2\pi/a|x|} \frac{du J_0(u)}{u^3} \right) \quad (\text{A28})$$

$$g(x) = \frac{a^2}{2\pi^2} + |x|^2 \left(A - \frac{1}{2} - A' \right) \quad (\text{A29})$$

here, $A = \int_{2\pi/L}^{2\pi/a} \frac{1-J_0(u)}{u^3} du \simeq 1.2$, $A' = \int_1^{2\pi/a|x|} \frac{J_0(u)}{u^3} du \simeq \int_0^\infty \frac{J_0(u)}{u^3} du \simeq 0.27$. Here, $a = 1$ is the lattice spacing.

$$g(x) = |x|^2 \times \mathcal{O}(0.01) \quad (\text{A30})$$

Hence, the orientation correlation function is given by,

$$C(x) \simeq \frac{1}{|x|^{\mathcal{B}}} e^{-|x|^2 \times \mathcal{O}(0.01) \times Ch_0^4} \quad (\text{A31})$$

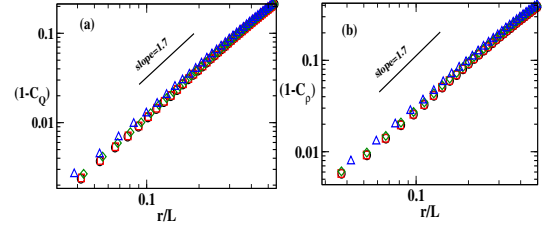


FIG. 6. (Color online) Cusp's exponent α (slope of the plot) for Q and ρ field. Different symbols used for different values of disorder strength: $h_0 = 0.0$ (circle), $h_0 = 0.05$ (square), $h_0 = 0.075$ (diamond), $h_0 = 0.10$ (triangle).

when measured on the scale of system size $N = K^2$, we get,

$$C_Q(N) \simeq \frac{1}{N^{\mathcal{B}'}} e^{-\mathcal{C}' h_0^4 N} \quad (\text{A32})$$

Here, $\mathcal{B}' = 1.17 \times 10^{-4}$ and $\mathcal{C}' = 3.9 \times 10^{-3}$.

Similarly, structure factor for density can be calculated using Eq. A18 and given by,

$$S_\rho(\mathbf{q}) = \gamma_1 \frac{h_0^4}{q^4} + \gamma_2 \frac{\Delta}{q^2} \quad (\text{A33})$$

where, $\gamma_1 = 0.5$ and $\gamma_2 = 0.4$ are constants and depends only on system parameters.

Appendix B: Morphology of domains: cusp exponent

Cusp Exponent: We also study the effect of disorder on the morphology of ordering domains. We calculate the behaviour of scaled two-point correlation functions $C_{Q,\rho}(r/L_{Q,\rho})$ for small $r/L_{Q,\rho}$. In the limit of small $r/L_{Q,\rho}$, $C_{Q,\rho}(r/L_{Q,\rho}) \sim 1 - (\frac{r}{L_{Q,\rho}})^\alpha$, where α is called the cusp exponent and features the domain morphology [30]. In Fig. 6 we plot the $1 - C_{Q,\rho}(r/L_{Q,\rho})$ vs. scaled distance $r/L_{Q,\rho}$ on log-log scale and estimate the cusp exponent α for both fields (Q, ρ). The exponent, $\alpha \simeq 1.7$ for both fields and for all disorder strengths. Hence domain morphology remains unaffected in the presence of disorder.